Redox Biology 45 (2021) 102021

Contents lists available at ScienceDirect

Redox Biology

journal homepage: www.elsevier.com/locate/redox

Elucidating the contribution of mitochondrial glutathione to ferroptosis in cardiomyocytes

Sehwan Jang [a,1], Xavier R. Chapa-Dubocq [a,1], Yulia Y. Tyurina [b], Claudette M. St Croix [c], Alexandr A. Kapralov [b], Vladimir A. Tyurin [b], Hülya Bayır [b,d], Valerian E. Kagan [b,e,f,g], Sabzali Javadov [a,*]

[a] Department of Physiology, University of Puerto Rico School of Medicine, San Juan, PR, 00936- 5067, USA
[b] Department of Environmental and Occupational Health, Center for Free Radical and Antioxidant Health, University of Pittsburgh, Pittsburgh, PA, 15260, USA
[c] Department of Cell Biology, University of Pittsburgh, Pittsburgh, PA, 15260, USA
[d] Department of Critical Care Medicine, University of Pittsburgh, and Children's Neuroscience Institute, UPMC Children's Hospital, Pittsburgh, PA, 15260, USA
[e] Department of Pharmacology and Chemical Biology, University of Pittsburgh, Pittsburgh, PA, 15260, USA
[f] Department of Chemistry, University of Pittsburgh, Pittsburgh, PA, 15260, USA
[g] Department of Radiation Oncology, University of Pittsburgh, Pittsburgh, PA, 15260, USA

ARTICLE INFO

Keywords:
Ferroptosis
Heart
Mitochondria
Glutathione
Oxidized phosphatidylethanolamine
Ischemia-reperfusion

ABSTRACT

Ferroptosis is a programmed iron-dependent cell death associated with peroxidation of lipids particularly, phospholipids. Several studies suggested a possible contribution of mitochondria to ferroptosis although the mechanisms underlying mitochondria-mediated ferroptotic pathways remain elusive. Reduced glutathione (GSH) is a central player in ferroptosis that is required for glutathione peroxidase 4 to eliminate oxidized phospholipids. Mitochondria do not produce GSH, and although the transport of GSH to mitochondria is not fully understood, two carrier proteins, the dicarboxylate carrier (DIC, *SLC25A10*) and the oxoglutarate carrier (OGC, *SLC25A11*) have been suggested to participate in GSH transport. Here, we elucidated the role of DIC and OGC as well as mitochondrial bioenergetics in ferroptosis in H9c2 cardioblasts. Results showed that mitochondria are highly sensitive to ferroptotic stimuli displaying fragmentation, and lipid peroxidation shortly after the onset of ferroptotic stimulus. Inhibition of electron transport chain complexes and oxidative phosphorylation worsened RSL3-induced ferroptosis. LC-MS/MS analysis revealed a dramatic increase in the levels of pro-ferroptotic oxygenated phosphatidylethanolamine species in mitochondria in response to RSL3 (ferroptosis inducer) and cardiac ischemia-reperfusion. Inhibition of DIC and OGC aggravated ferroptosis and increased mitochondrial ROS, membrane depolarization, and GSH depletion. Dihydrolipoic acid, an essential cofactor for several mitochondrial multienzyme complexes, attenuated ferroptosis and induced direct reduction of pro-ferroptotic peroxidized phospholipids to hydroxy-phospholipids *in vitro*. In conclusion, we suggest that ferroptotic stimuli diminishes mitochondrial bioenergetics and stimulates GSH depletion and glutathione peroxidase 4 inactivation leading to ferroptosis.

1. Introduction

Ferroptosis is a recently discovered iron-dependent programmed cell death that occurs due to excessive oxygenation of polyunsaturated fatty acid residues of phospholipids by non-heme iron-containing lipoxygenases (LOX), particularly 15-lipoxygenase (15LOX), and by the insufficient capacity of a selenoprotein glutathione peroxidase 4 (GPX4) to eliminate oxidized phospholipids [1,2]. Among thousands of molecular species of oxidizable phospholipids, only four phospholipids (two of each), arachidonoyl- and adrenoyl-phosphatidylethanolamines (PEs) have been shown to serve as substrates for 15LOX to produce pro-ferroptotic hydroperoxy-PE signals [3,4]. Normally, GPX4 reduces peroxidized PEs to stable hydroxy-PEs at the expense of reduced glutathione (GSH) oxidation. GSH, a GPX4 cofactor, is produced from cysteine provided by the cystine/glutamate antiporter system x_c^- in the plasma membrane; inhibition of cystine import/GSH synthesis diminishes GPX4 function and leads to ferroptosis [1,5].

* Corresponding author.
E-mail address: sabzali.javadov@upr.edu (S. Javadov).
[1] These authors contributed equally to this work.

https://doi.org/10.1016/j.redox.2021.102021
Received 14 April 2021; Received in revised form 17 May 2021; Accepted 20 May 2021
Available online 1 June 2021

Abbreviations

BMA	butylmalonic acid
CD	cysteine deprivation
DHLA	dihydrolipoic acid
DIC	dicarboxylate carrier
Fer-1	ferrostatin-1
GPX4	glutathione peroxidase 4
GSH	reduced glutathione
GSSG	glutathione disulfide (oxidized glutathione)
IMM	inner mitochondrial membrane
IR	ischemia-reperfusion
KGDH	α-ketoglutarate dehydrogenase
LDH	lactate dehydrogenase
15LOX	15-lipoxygenase
LVDP	left ventricular developed pressure
mtROS	mitochondrial ROS
OGC	oxoglutarate carrier
OXPHOS	oxidative phosphorylation
PDH	pyruvate dehydrogenase
PSA	phenylsuccinic acid
PE	phosphatidylethanolamine
PEox	oxidized PE
ROS	reactive oxygen species
TCA	tricarboxylic acid
TMRM	tetramethylrhodamine, methyl ester
XJB	XJB-5-131

Due to their central role in cell metabolism, redox status, and bioenergetics, recent studies suggested a pivotal role of mitochondria in ferroptosis, particularly, in high-energy consuming organs such as the heart. Ferroptotic cells contain dense and compact mitochondria where cristae are mostly lost or disorganized, and the outer mitochondrial membrane is ruptured [2,6]. Human fibrosarcoma HT-1080 cells depleted of mitochondria by Parkin-dependent mitophagy demonstrated high resistance to ferroptosis induced by cystine deficiency [7]. Ferroptosis induced by cysteine deprivation (CD) has been shown to require glutaminolysis (conversion of glutamine to glutamate), a major source of anaplerosis, which fuels the tricarboxylic acid (TCA) cycle in mitochondria through the α-ketoglutarate dehydrogenase (KGDH) complex [8]. KGDH participates not only in the regulation of glutamate levels but also serves as a redox sensor to maintain mitochondrial redox status [9,10]. It is a major source of mitochondrial ROS (mtROS) and can produce eight times more ROS than complex I [11]. KGDH as well as other mitochondrial 2-ketoacid dehydrogenases such as pyruvate dehydrogenase (PDH) and branched-chain ketoacid dehydrogenase contain lipoic acid (LA), a cofactor covalently attached by an amide bond to a terminal lysine residue of E2 subunit in these enzymes. Also, LA and its reduced form dihydrolipoic acid (DHLA) are strong biological antioxidants [12] that act as metal chelators and reducers of the oxidized forms of other antioxidants such as thioredoxin, and vitamins C and E.

GSH is synthesized from its constituent amino acids exclusively in the cytosol however it is also localized in the endoplasmic reticulum, nucleus, and mitochondria to maintain the redox status [13,14]. Mitochondria contain 10–15% of total cellular GSH although the concentration of mitochondrial GSH is similar to the cytosol. Inner mitochondrial membrane (IMM) is impermeable to GSH and therefore, a specific transport mechanism(s) is required for the transport of GSH across the membrane [15,16]. Studies in isolated kidney mitochondria revealed that over 80% of GSH is transported to the matrix by the dicarboxylate carrier (DIC) and the oxoglutarate carrier (OGC) [17,18]. However, other studies questioned the role of these carrier proteins in mitochondrial GSH transport [19]. DIC (*Slc25a10*) and OGC (*Slc25a11*) are two of eight known anion carriers that transport dicarboxylates (malonate, malate, and succinate) across the IMM in exchange for phosphate, sulfate, and thiosulfate (DIC) or 2-oxoglutarate for dicarboxylates (OGC). These transporters are important for the maintenance of mitochondrial bioenergetics, particularly, TCA cycle, as well as other metabolic processes such as fatty acid synthesis [20]. The role of the DIC and OGC in ferroptotic cell death remains unknown.

In the present study, we elucidated the role of mitochondria, particularly, mitochondrial GSH, in response to ferroptotic stimuli in cardiomyocytes and pharmacological inhibition of DIC and OGC on mitochondrial function and cell survival. We suggested that mitochondrial GSH and redox status are involved in the regulation of ferroptotic signaling, and DHLA can exert anti-ferroptotic effects. Our results demonstrate that mitochondrial bioenergetics and GSH play a major role in ferroptotic cell death.

2. Materials and methods

2.1. Cell culture

H9c2 embryonic rat cardioblastic cells were cultured according to the manufacturer's recommendations (ATCC, Manassas, VA). Briefly, the cells were cultured in DMEM based modified media containing 4 mM L-glutamine, 4.5 g/L glucose, 1 mM sodium pyruvate, and 1.5 g/L sodium bicarbonate supplemented with 10% fetal bovine serum and 1% antibiotic solution (HyClone) and maintained in 95% air and 5% CO_2 at 37 °C. Cells maintained within 80–90% confluence from passages 3–10 were used for experiments. All chemicals were purchased from Sigma-Aldrich (St. Louis, MO).

2.2. Cell death assay

H9c2 cells were seeded to 70–80% confluence a day before the assay. After treatment with inhibitors, the cells were maintained in 95% air and 5% CO_2 at 37 °C. To measure cell death, the Alamarblue® assay was used as per the manufacturer's recommendations (Thermo Fisher Scientific). In addition, lactate dehydrogenase (LDH) activity in the incubation medium was measured to estimate cell death [21]. Ferrostatin-1 (Fer-1, an inhibitor of ferroptosis), carbonyl cyanide m-chlorophenylhydrazone (CCCP), an oxidative phosphorylation (OXPHOS) uncoupler, and inhibitors for ETC complexes, OXPHOS, and adenine nucleotide translocase were added at the same time as the pro-ferroptotic compound RSL3 whereas DHLA was added to the culture medium 1 h before stimulation of ferroptosis. To inhibit DIC and OGC, the cells were incubated for 24 h in a serum-free medium containing 5 mM butylmalonic acid (BMA, a DIC inhibitor) and/or 5 mM phenylsuccinic acid (PSA, an OGC inhibitor).

2.3. Cardiac ischemia-reperfusion

Male adult Sprague Dawley rats (275–325 g) were purchased from Taconic (Hillside, NJ). All experiments were performed according to protocols approved by the UPR Medical Sciences Campus Institutional Animal Care and Use Committee and conformed to the National Research Council Guide for the Care and Use of Laboratory Animals published by the US National Institutes of Health (2011, 8th edition). All chemicals were handled with the appropriate personal protective equipment under the regulations established by the Biosafety and Biosecurity Committee of the UPR Medical Sciences Campus. Hearts were isolated from the rats and perfused according to the Langendorff-mode

technique as described previously [22].

To induce *ex-vivo* cardiac ischemia-reperfusion (IR), the hearts were initially perfused for 20 min to stabilize cardiac function (equilibration period), and then, were subjected to global ischemia for 25 min followed by 60-min reperfusion in the presence or absence of Fer-1 and XJB-5-131 (XJB, a mitochondria-targeted ROS and electron scavenger). Animals were randomly assigned to the following 4 groups: i) control (no IR, n = 6), ii) IR (n = 8), iii) IR + Fer-1 (n = 8), and iv) IR + XJB (n = 7). Fer-1 (1 μM) and XJB (0.2 μM) dissolved in DMSO were present in the perfusion buffer 10 min before ischemia and throughout the entire reperfusion period. A water-filled balloon inserted into the left ventricle (LV) and connected to a pressure transducer was used to measure cardiac function. Functional parameters including heart rate (HR), the rate of contraction and relaxation (±dP/dt), aortic pressure, LV systolic pressure (LVSP), and end-diastolic pressure (LVEDP) were continuously monitored using the Labscribe2 Data Acquisition Software (iWorx 308T, Dover, NH, USA). LV developed pressure (LVDP) was calculated as the difference between LVSP and LVEDP (LVDP = LVSP-LVEDP). To estimate cell death, LDH activity was measured in the coronary effluent during the reperfusion period. XJB was provided by Dr. Peter Wipf (University of Pittsburgh, PA).

2.4. LC-MS/MS analysis of phospholipids

Lipids were extracted using the Folch procedure, and phosphorus was determined by a micro-method as described previously [3]. Phospholipids were analyzed by LC/MS using a Dionex Ultimate 3000 HPLC system coupled on-line to the Orbitrap Fusion Lumos mass spectrometer (Thermo Fisher Scientific) using a normal phase column (Luna 3 μm Silica (2) 100 Å, 150 × 2.0 mm, (Phenomenex)) as described previously [3].

2.5. Lipid peroxidation imaging

To visualize lipid peroxidation, cells were seeded in glass-bottom tissue culture dishes (35-mm, MatTek Corp) and prestained with MitoTracker® Deep Red FM (50 nM) and Liperfluo (10 μM, Dojindo Molecular Technologies Inc.,) for 30 min and then, RSL3 (0.5 μM), and/or Fer-1 (2 μM) were added, and the cells were incubated for an additional 1 h. The cells were washed twice with PBS, and then the dish was inserted into a closed, thermo-controlled (37 °C) stage top incubator (Tokai Hit Co.) above the motorized stage of an inverted Nikon TiE fluorescent microscope equipped with a 60x optic (Nikon, CFI Plan Fluor, NA 1.4). Liperfluo was excited using a diode-pumped light engine (SPECTRA X, Lumencor) and detected using an ORCA-Flash 4.0 sCMOS camera (Hamamatsu) and excitation and emission filters from Chroma. Data were collected on approximately 10–20 cells per stage position, with 10–15 stage positions per condition. Data was collected and analyzed using NIS Elements (Nikon Inc. Melville, NY).

2.6. Mitochondrial fragmentation assay

The cells were live stained with 50 nM MitoTracker® Deep Red FM for 1 h, and then, RSL3 (0.5 μM), and/or Fer-1 (2 μM) were added, and the cells were incubated in a humidified incubator containing 95% air and 5% CO_2 at 37 °C for an additional 1 h. Images of live cells were captured using a Nikon Ti inverted microscope (Nikon Inc.). After out-of-focus signals were excluded, images were thresholded and underwent object-based particle analysis using ImageJ [23]. Whole images were used to calculate the percent of fragmented mitochondria. Circularity greater than 0.9 was considered fragmented.

2.7. Western blotting

To analyze expression levels, proteins were separated by SDS-PAGE and identified by Western blotting [24]. The membranes were immunoblotted with antibodies against DIC (Millipore MABN457), OGC (Santa Cruz Biotech sc-515593), ATP5A (Mitochondrial ATP synthase subunit alpha, Abcam ab14748), prelamin-A/C (LMNA, Abcam, ab108595), alpha-tubulin (TUBA, Abcam ab7291), beta-actin (ACTB, Abcam, ab6276) and GPX4 (Abcam, ab125066) followed by IRDye® secondary antibodies (LI-COR Biosciences, Lincoln, NE, USA) per the manufacturer's recommendations. Membranes were scanned using ODYSSEY® CLx imager (LI-COR). The resulting images were analyzed with Image Studio Lite (LI-COR) and ImageJ [23].

2.8. Mitochondrial membrane potential ($\Delta\Psi_m$) and mtROS

Live cells were stained with tetramethylrhodamine, methyl ester (TMRM, Sigma), MitoSOX Red, MitoTracker™ Green FM (Thermo), and Hoechst 33342 (Sigma) for visualization of $\Delta\Psi_m$, mtROS, mitochondria, and nucleus, respectively, as described previously [25]. Images were captured using Olympus IX73 microscope with DP73 camera controlled by Cellsense Dimension (Olympus) software in quantification mode. For quantification of fluorescence intensity, integrated pixel densities from red channels (TMRM or MitoSOX) were normalized to cell numbers calculated from the object-based count of the nucleus. ImageJ [23] was used for image analysis and compositions.

2.9. Assessment of the capacity of DHLA to reduce PEox in vitro

To assess the capability of DHLA to reduce hydroperoxy-eicasotetraenoyl-PE (HpETE-PE) to hydroxyeicasotetraenoyl-PE (HETE-PE) *in vitro*, 25 μM HpETE-PE was incubated in 50 μL of 20 mM HEPES buffer (pH 7.4) containing 100 μM diethylenetriamine pentaacetate (DTPA, a Fe^{3+} chelator) in the presence and absence of different concentration of DHLA (at ratio 0–20 of DHLA/HpETE) for 20 min at room temperature. Lipids were extracted by Folch procedure and LC-ESI-MS/MS analysis was performed using a Dionex Ultimate 3000 HPLC system coupled online to a linear ion-trap mass spectrometer (LXQ, ThermoFisher Scientific) or Q-Exactive hybrid quadrupole-orbitrap mass spectrometer (ThermoFisher Scientific) using a C30 column (Thermo Acclaim 2.1 mm × 150 mm) in the gradient of solvents A (acetonitrile/water, 45:5) and B (2-propanol/water, 45:5v/v), containing 5 mM ammonium acetate at a flow rate of 150 μL/min. Spectra were acquired in negative-ion mode using a spray voltage of 5.0 kV and a capillary temperature of 150 °C for detection of HpETE-PE (m/z798) and HETE-PE (m/z782).

2.10. GSH imaging and quantitative analysis of GSH levels

For imaging, live cells were stained with Thiol Fluorescent Probe IV (Calbiochem) and MitoTracker Green FM (Thermo-Fisher) per the manufacturer's recommendations. Live images were acquired by Olympus IX73 microscope. ImageJ was used for image compositions. GSH levels were measured in harvested cells or mitochondria. Mitochondria were isolated from H9c2 cells as described previously [25]. To measure GSH, harvested cells or isolated mitochondria were homogenized with 20% (w/v) glass beads (710–1180 μm size) in PBS for 20 min at 4 °C. After the homogenization, the samples were centrifuged at 20, 000×g for 20 min at 4 °C, and the supernatant was collected and used for the analysis of GSH. 1–10 μM GSH were used as standards. The concentrations of GSH were normalized to protein quantified by Bradford protein assay (Bio-Rad). CLARIOstar microplate reader (BMG Labtech) was used for measurements.

2.11. Statistical analysis

Data were analyzed using ANOVA with normality test (Shapiro-Wilk) and pairwise multiple comparison procedures (Holm-Sidak method), in addition to Student's t-test. Results are presented as mean ± SE. $p < 0.05$ was considered statistically significant.

3. Results

3.1. Responses of mitochondria to ferroptotic stimuli in cardiomyocytes

First, we evaluated the effects of RSL3 on cell survival 18 h after treatment with the ferroptosis inducers. As shown in Fig. 1, increases in the concentration of RSL3 enhanced cell death which reached the maximum (97%) at 0.5 μM RSL3-induced cell death was completely prevented in the presence of 2 μM Fer-1.

We assessed the effects of RSL3 on mitochondrial morphology, lipid peroxidation, and ferroptotic PEox levels at 1 h after treatment. RSL3 induced lipid peroxidation in mitochondria as evidenced by increased intensity of Liperfluo, a fluorescence dye used for specific detection of lipid peroxides (Fig. 2A). Peroxidation of lipids was markedly reduced in cells treated with RSL3 in the presence of Fer-1. Enhanced lipid peroxidation was associated with mitochondrial fragmentation; RSL3 induced a 1.9-fold increase in the number of fragmented mitochondria that was attenuated in the presence of Fer-1 (Fig. 2B). Next, we analyzed PEox species and their non-oxidized precursors in cell lysates, cytosol, and mitochondria isolated from control, Fer-1, RSL3 and RSL3+Fer-1 treated H9c2 cells by LC-MS/MS (Fig. 2C and D). Results demonstrated that RSL3 significantly increased the levels of major species of hydroperoxy-PE (PE-OOH) containing arachidonoyl- and adrenoyl acyls such as PE (36:4)-OOH, PE(38:4)-OOH, and PE(40:4)-OOH in cardiomyocytes as early as 1 h after treatment. Importantly, accumulation of the PEox species was observed in mitochondria indicating an early response of these organelles to ferroptotic stimuli. Accumulation of the PEox signals was prevented by Fer-1 (Fig. 2D). Thus, ferroptotic death in cardiomyocytes is characterized by accumulation of peroxidized PEs species and fragmentation of mitochondria.

3.2. ETC and OXPHOS are involved in ferroptosis

In the next set of experiments, we sought to investigate whether mitochondrial bioenergetics, particularly, ETC and OXPHOS are involved in ferroptosis. Treatment of the cells with inhibitors for individual ETC complexes and OXPHOS for 18 h affected cell death differently in RSL3 (30 nM) treated cardiomyocytes (Fig. 3). Particularly, inhibition of complexes I and III in the presence of RSL3 induced a 6-fold increase in cell death compared to the control (RSL3 only treated) cells. Among RSL3-treated groups, maximum cell death was observed in the presence of oligomycin, which induced a 15.6-fold increase in cell death. Moreover, inhibition of adenine nucleotide translocase, an exchanger responsible for the transport of ATP from the matrix to the intermembrane space, also significantly (~6-fold) aggravated cell death induced by RSL3. Likewise, RSL3-induced cell death was further worsened by 2.7-fold ($p < 0.05$) by CCCP, an OXPHOS uncoupler, compared to control. Inhibition of complexes II and IV had no significant effects on RSL3-induced cell death (Fig. 3). Altogether, the results of these experiments demonstrate that mitochondrial bioenergetics is involved in ferroptosis.

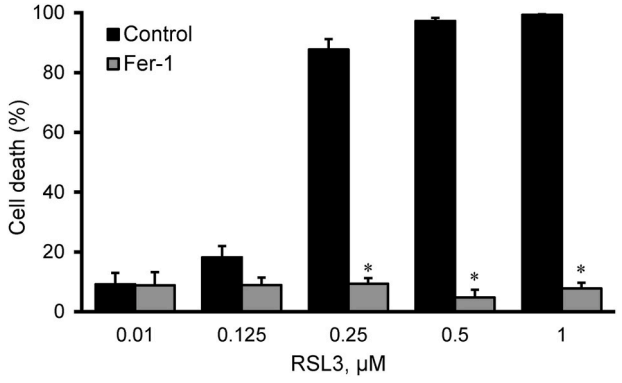

Fig. 1. Ferroptosis in H9c2 cardioblasts induced by RSL3. The cells were incubated with RSL3 for 18 h in the presence or absence of 2 μM ferrostatin-1 (Fer-1). Cell death was calculated from the measurements by the AlamarBlue Cell Viability Assay. *$p < 0.01$ vs. control. n = 3 per group.

3.3. DIC and OGC inhibitors aggravate whereas DHLA attenuates ferroptosis

Next, we examined the effects of inhibition of DIC and OGC on ferroptotic cell death. Western blot analysis of DIC and OGC expression demonstrated that the mitochondria isolated from H9c2 cardioblasts contain a high amount of both transporters (Fig. 4A). PSA (DIC inhibitor, 5 mM) and/or BMA (OGC inhibitor, 5 mM) enhanced the sensitivity of the cells to RSL3 (Fig. 4B and C). Particularly, BMA increased RSL3-induced cell death by 34% and 37% ($p < 0.05$ for both) whereas PSA induced a 55% and 22% increase in cell death following 6 h and 9 h, respectively. The combination of PSA and BMA did not exert any additive/synergistic effects at both time points. Additional cell death induced by the inhibitors in RSL3-treated cells was attributed to ferroptosis as the cell death was inhibited by Fer-1 up to 86% under all treatment conditions (Fig. 4B and C).

These data suggest that inhibition of DIC and OGC might affect mitochondrial bioenergetics and redox status to aggravate ferroptosis in H9c2 cardioblasts. Hence, we next investigated whether DHLA, a reduced form of LA containing two thiol groups, could prevent ferroptotic cell death induced by RSL3. Our concentration-dependent studies showed that DHLA does not exert anti-ferroptotic effects in cardiomyocytes at concentrations lower than 25 μM (*results not shown*). However, pretreatment with 25 μM and 100 μM DHLA markedly attenuated RSL3-induced cell death, and the extent of the anti-ferroptotic effects was comparable with that induced by Fer-1 (Fig. 5A). We also investigated the capability of DHLA to reduce the pro-ferroptotic HpETE-PE to HETE-PE *in vitro*. Results LC-MS analysis of HpETE-PE (*m/z* 798) and HETE-PE (*m/z* 782) in control (Fig. 5B) or DHLA-treated (Fig. 5C) samples demonstrated that DHLA significantly decreased HpETE-PE levels concurrent with increased HETE-PE. Concentration-dependence analysis of the HpETE-PE reduction and HETE-PE revealed a close relationship between HpETE-PE and HETE-PE in the presence of DHLA where reduced levels of HpETE-PE were associated with a concurrent increase of HETE-PE levels and *vice versa* (Fig. 5D). These data provide direct evidence of the capability of DHLA to reduce pro-ferroptotic PEox species to hydroxy-PEs.

3.4. Inhibition of DIC and OGC increases ROS and reduces GSH in mitochondria

Next, we investigated whether inhibition of DIC or OGC affects $\Delta\Psi_m$ and mtROS production and modulates the redox status of the cells. BMA (5 mM) or PSA (5 mM) applied individually had no significant effects on the $\Delta\Psi_m$ which was reduced only 9% compared to untreated cells (Fig. 6A). However, the cells treated with BMA in combination with PSA displayed 14% less ($p < 0.05$ vs. control) $\Delta\Psi_m$ than control cells. Analysis of mtROS by mitoSOX in cells revealed, respectively, a 45% and 54% ($p < 0.01$ vs. control for both) increase in the presence of BMA and PSA (Fig. 6B). Simultaneous incubation of the cells with both inhibitors further increased mtROS production that was 98% ($p < 0.05$) more compared to the control group.

In the next set of experiments, we determined cellular and mitochondrial GSH levels in RSL3-treated H9c2 cells in the presence or absence of PSA, BMA, and their combination. To visualize GSH in mitochondria, the cells were incubated Thiol Fluorescent Probe IV and Mitotracker™ (Fig. 7A). Quantification of GSH in cell lysates showed that incubation of the cells with 0.5 μM RSL3 for 1 h induced a 13% ($p < 0.01$) decrease of cellular GSH (Fig. 7B and C). Analysis of isolated mitochondria revealed high sensitivity of GSH to RSL3; GSH levels in mitochondria were decreased by 33% ($p < 0.01$) after 1-h treatment.

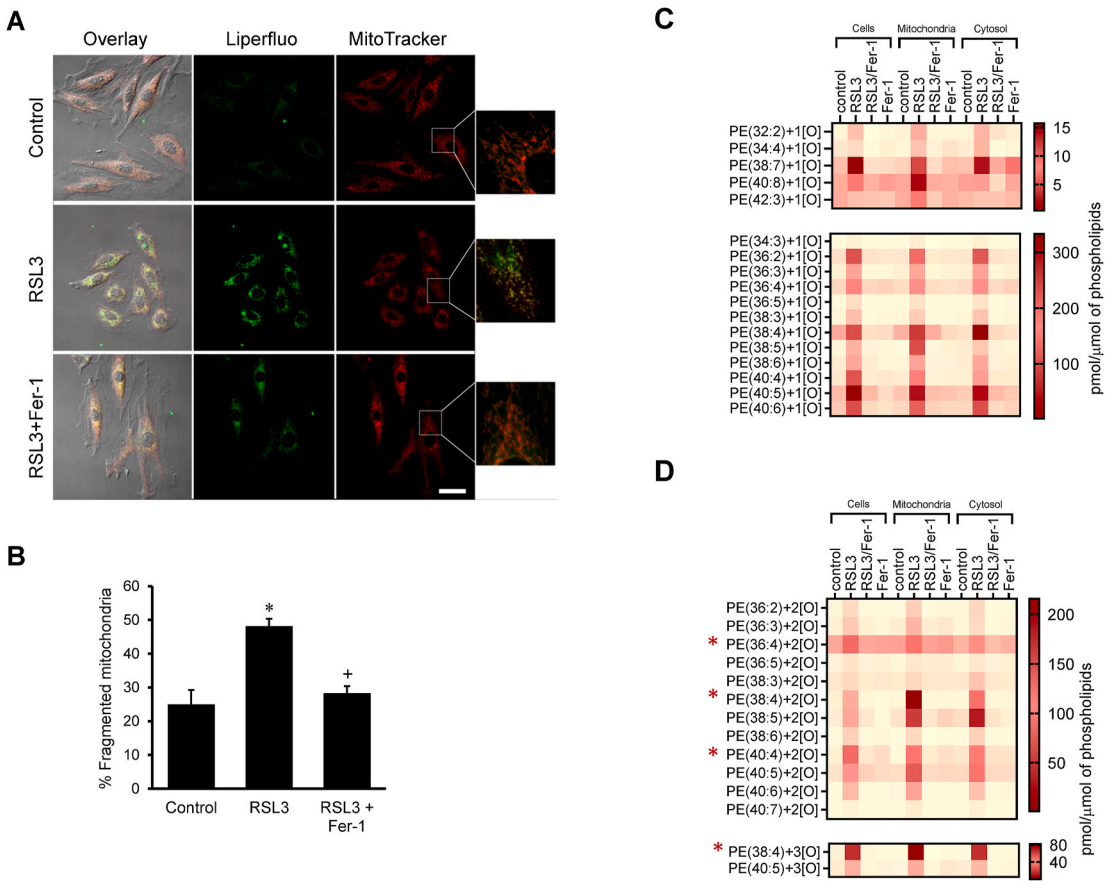

Fig. 2. The effects of RSL3 on mitochondrial lipid peroxidation, fragmentation, and peroxidized PE species in H9c2 cardiomyocytes. ***A***, To visualize peroxidized lipids, the cells were seeded in glass-bottom tissue culture dishes (35-mm, MatTek Corp) and prestained with MitoTracker® Deep Red FM (50 nM) and Liperfluo (10 μM, Dojindo Molecular Technologies Inc.,) for 30 min and then, RSL3 (0.5 μM), and/or Fer-1 (2 μM) were added, and the cells were incubated for an additional 1 h. The cells were washed twice with PBS, and then the dish was inserted into a closed, thermo-controlled (37 °C) stage top incubator (Tokai Hit Co.) above the motorized stage of an inverted Nikon TiE fluorescent microscope equipped with a 60x optic (Nikon, CFI Plan Fluor, NA 1.4). Liperfluo was excited using a diode-pumped light engine (SPECTRA X, Lumencor) and detected using an ORCA-Flash 4.0 sCMOS camera (Hamamatsu) and excitation and emission filters from Chroma. Data were collected on approximately 10–20 cells per stage position, with 10–15 stage positions per condition. Data was collected and analyzed using NIS Elements (Nikon Inc. Melville, NY). Zoomed and enhanced images are shown beside each image. Bar = 50 μm. ***B***, To analyze fragmentation of mitochondria, the cells were stained using 50 nM MitoTracker® Deep Red FM for 1 h, then incubated for an additional 1 h with 0.5 μM RSL3 with or without 2 μM Fer-1. Control cells were stained in the culture medium containing 0.01% DMSO. Images of live cells were captured using a Nikon Ti inverted microscope (Nikon Inc.). After out-of-focus signals were excluded, individual mitochondria were analyzed in thresholded images using ImageJ. A total of 71191 objects were analyzed to calculate the percent of fragmented mitochondria. Circularity greater than 0.9 was considered fragmented. $^{*}p < 0.05$ vs. control, $^{+}p < 0.01$ vs. RSL3. n = 3 per group. ***C, D,*** Heat maps of peroxidized PE species analyzed by LC-MS in cell lysates, mitochondria, and cytosol isolated from control cells and the cells treated with 0.5 μM RSL3 for 1 h in the presence or absence of 2 μM Fer-1. (For interpretation of the references to colour in this figure legend, the reader is referred to the Web version of this article.)

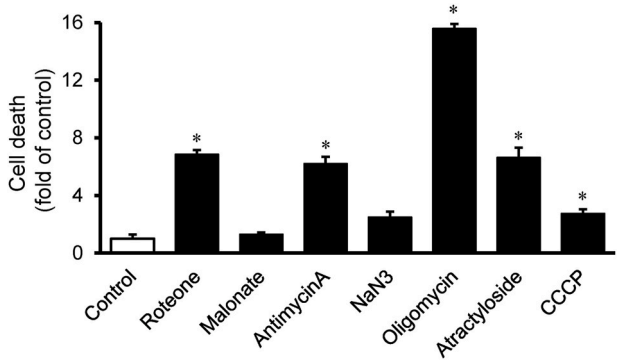

Fig. 3. The effects of inhibitors of individual ETC complexes and OXPHOS on ferroptosis. The cells were treated with 30 nM RSL3 in the presence or absence of mitochondrial inhibitors for 18 h. The inhibitors were added simultaneously with RSL3. Data are presented as fold changes of control (RSL3 alone). $^{*}p < 0.05$ vs. control. n = 4 per group.

These data are consistent with our previous studies wherein GSH levels measured with high accuracy by the gas cluster ion beam secondary ion mass spectrometry imaging technique were significantly decreased in H9c2 cells after treatment with 0.5 μM RSL3 for 2.5 h [26]. Fer-1 had no significant effects on both cellular and mitochondrial GSH. Inhibition of DIC and OGC in the absence of RSL3 reduced the GSH level in mitochondria by 20% ($p < 0.01$) and 26% ($p < 0.01$), respectively. However, RSL3 had no significant effects on the GSH reductions induced by the inhibitors. We have previously shown that 1 μM RSL3 markedly reduces the GPX4 protein level in HT-1080 cancer cells after 10-h treatment [27]. In the present study, incubation of the H9c2 cardiomyocytes with 0.5 μM RSL3 for 1 h did not affect cellular GPX4 levels but reduced it 17% ($p > 0.05$) in mitochondria (Fig. 7D). This can be explained by a low RSL3 concentration and shorter incubation time. Thus, the results demonstrate that inhibition of DIC and OGC decreases mitochondrial GSH levels associated with increased mtROS in control cells.

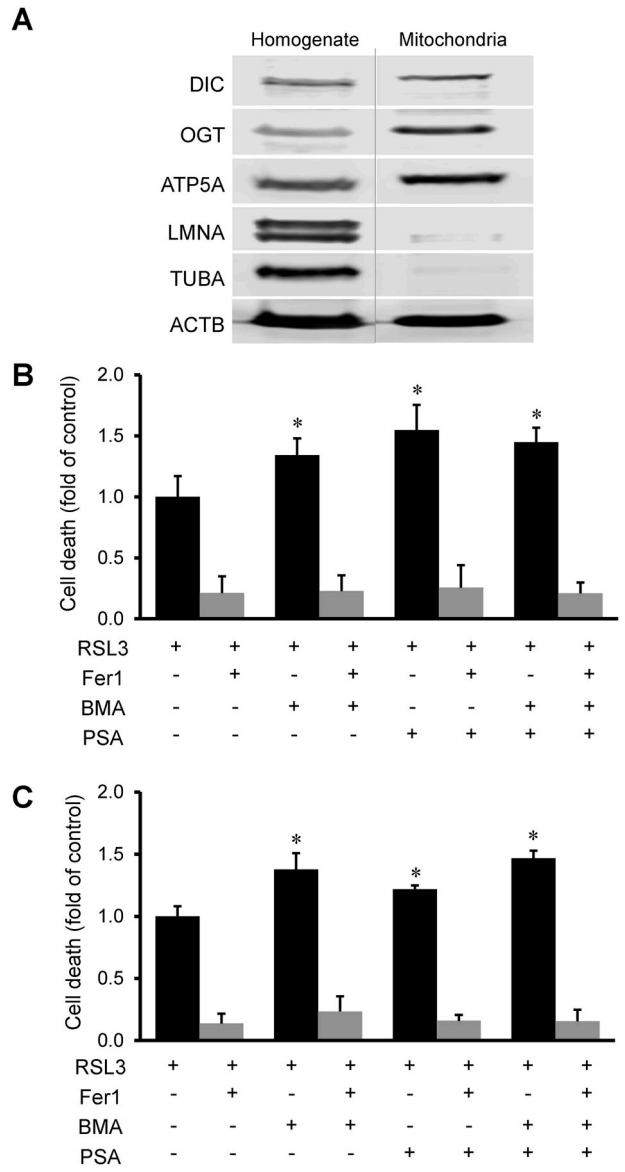

Fig. 4. The effects of DIG and OGC inhibition on RSL3-induced cell death. ***A,*** Protein levels of DIG and OGC. DIC and OGC immunoblots are shown in cell homogenate and isolated mitochondria. ATP synthase subunit alpha (ATP5A), prelamin A/C (LMNA), and tubulin alpha chain (TUBA) were used as the markers for the mitochondria, nucleus, and cytoplasm, respectively. β-Actin (ACTB) was used as a loading control. ***B, C,*** The cells were exposed to 0.5 μM RSL3 for 6 h (***B***) or 9 h (***C***) in the presence or absence of the DIC inhibitor butylmalonic acid (BMA, 5 mM) and/or OGC inhibitor phenylsuccinic acid (PSA, 5 mM). Grey bars represent the cells exposed to RSL3 that were treated with 2 μM Fer-1 in the presence of BMA and/or PSA. Cell death was measured as LDH release normalized by cell number and presented as a fold change of control. *$p < 0.05$ vs. control.

3.5. Cardiac IR induces accumulation of ferroptotic PE species in mitochondria

To examine whether mitochondria are directly involved in ferroptosis in response to cardiac IR, isolated rat hearts were subjected to *ex-vivo* IR in the presence or absence of Fer-1 or the mitochondria-targeting ROS scavenger, XJB. We have previously shown the cardioprotective effects of XJB against IR injury in adult [21] and aged rat hearts [28]. Furthermore, XJB exhibited anti-ferroptotic effects by preventing erastin- or RSL3-induced cell death in HT-1080 fibrosarcoma cells [29]. Cardiac IR significantly diminished post-ischemic recovery of untreated

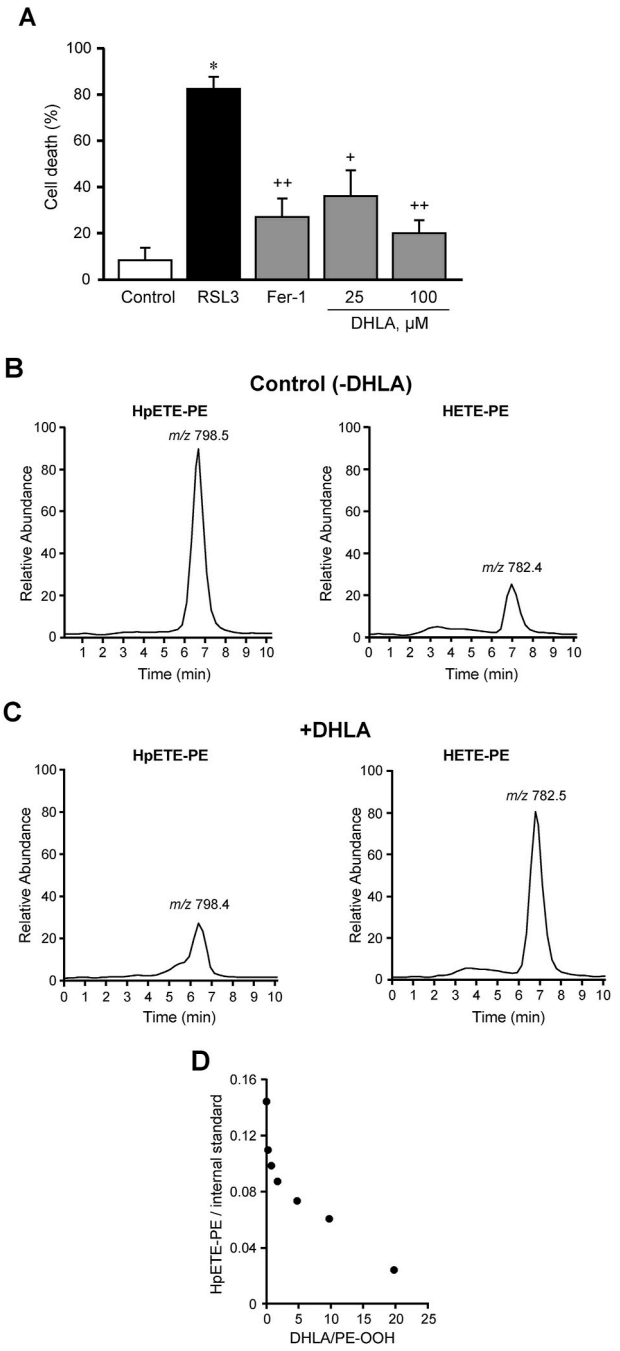

Fig. 5. Anti-ferroptotic effects of DHLA. ***A***, Ferroptosis was induced in H9c2 cardiomyocytes by 125 nM RSL3 in the presence or absence of Fer-1 (2 μM) or DHLA (75 and 300 μM). *$p < 0.01$ vs. control, +$p < 0.05$, $^{++}p < 0.01$ vs. RSL3. n = 3–4 per group. ***B,C,D***, LC-MS/MS analysis of the reduction of the pro-ferroptotic hydroperoxy-eicasotetraenoyl-PE (HpETE-PE) to hydroxyeicasotetraenoyl-PE (HETE-PE) by DHLA *in vitro*. Incubation of HpETE-PE with/without DHLA (HpETE-PE to DHLA ratio is 1:5) was performed in 20 mM HEPES buffer (pH 7.4) with 100 μM diethylenetriamine pentaacetate (a Fe^{3+} chelator). HpETE-PE (*m/z*798) and HETE-PE (*m/z*782) levels were analyzed by LC-MS in control (***B***) and DHLA-treated (***C***) samples, and concentration-dependence of the HpETE-PE reduction to HETE-PE by DHLA was calculated (***D***).

hearts (Fig. 8A) that showed only a 26% recovery of LVDP concurrent with the reduced cardiac work at 60-min of reperfusion. Fer-1 and XJB improved recovery of cardiac function after ischemia as evidenced by a 66% and 56% ($p < 0.05$ vs. IR for both) recovery of LVDP by the end of

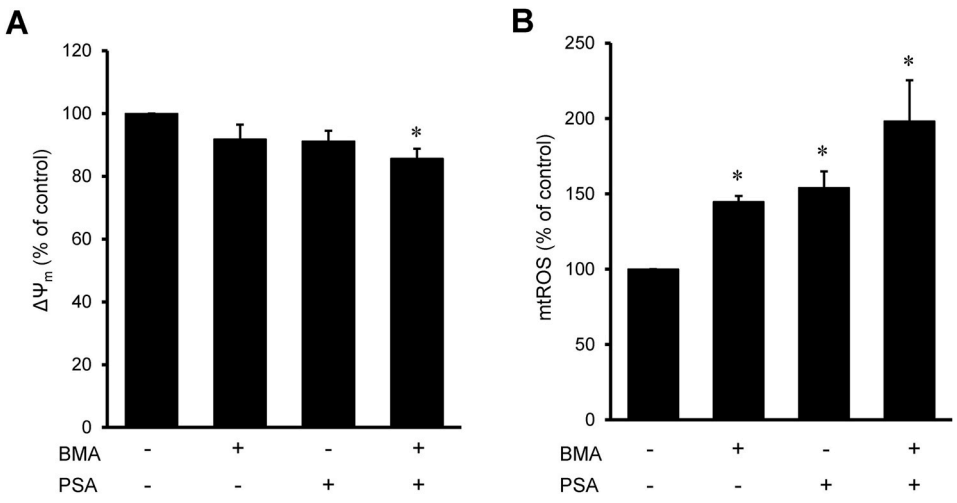

Fig. 6. Mitochondrial membrane potential ($\Delta\Psi_m$) and mtROS cells treated with DIG and OGC inhibitors. H9c2 cells were live stained with fluorescence dyes for visualization of $\Delta\Psi_m$ (50 nM TMRM for 1 h, ***A***) or mtROS (2 μM MitoSOX for 15 min, ***B***) in the presence of 50 nM Hoechst 33342 (for nuclear staining) for 1 h. The cells were incubated with 5 mM BMA and/or 5 mM PSA for 24 h. Integrated pixel intensities from TMRM or MitoSOX signals were normalized by cell number which was calculated from Hoechst 33342 staining. *$p < 0.05$ vs. control; n = 3 per group.

reperfusion, respectively. In addition, Fer-1 and XJB decreased IR-induced cell death in the heart; the activity of LDH released from the Fer-1- and XJB-treated hearts was, respectively, 3.2 and 3.3 folds less ($P < 0.05$ vs. IR for both) in comparison with untreated hearts (Fig. 8B). Analysis of the ferroptotic PEox species, PE(38:4)-OOH and PE (40:4)-OOH by LC-MS/MS in mitochondria isolated from control and IR hearts revealed a 60% ($P < 0.05$) and 107% ($P < 0.05$) increase of PE (38:4)-OOH and PE(40:4)-OOH, respectively, compared to control hearts (Fig. 8C). However, treatment with Fer-1 and XJB decreased the accumulation of the PEox species in mitochondria. These data demonstrate that ferroptotic cell death is involved in IR-induced cardiac dysfunction and mitochondria participate in ferroptotic death signaling and produce ferroptotic PEox species in IR hearts.

4. Discussion

In the present study, we examined the contribution of mitochondrial GSH to ferroptotic cell death. First, we confirmed the specificity of ferroptotic cell death in H9c2 cardioblastic cells when RSL3-induced cell death was prevented by Fer-1. Second, we revealed an early response of cardiac mitochondria to ferroptosis that were found mostly fragmented 1 h after RSL3 treatment. Notably, RSL3 induced accumulation of ferroptotic PEox species in cardiomyocytes, particularly, in mitochondria. Likewise, accumulation of PEox species was observed in mitochondria of hearts exposed to *ex-vivo* IR. Third, inhibition of DIC and OGC, the carrier proteins that transfer dicarboxylates and are known as potential GSH transporters, decreased GSH levels in mitochondria, increased mtROS and $\Delta\Psi_m$ loss, and aggravated RSL3-induced cell death. Fourth, DHLA significantly reduced ferroptotic cell death.

By applying the gas cluster ion beam secondary ion mass spectrometry imaging technique with 1.2 μm spatial resolution to map PE and PEox, we have recently demonstrated accumulation of major ferroptotic PEox in H9c2 cardiomyocytes [26]. Significant increases in the level of major ferroptotic PEox species in mitochondria as early as 1 h following incubation with RSL3 provide strong evidence on the early response of mitochondria to ferroptotic signaling. We have previously detected these species in subcellular compartments including endoplasmic reticulum, mitochondria, and mitochondria-associated membranes, where they may exist as individual molecules, clusters, or protein adducts and compromise the integrity of the plasma membrane [3,30]. Obtained results demonstrated, that free DHLA prevented RSL3-induced ferroptosis in H9C2 cells (Fig. 5A). The anti-ferroptotic effect of free DHLA can be explained by its antioxidant properties and normalizing effect on GSH. DHLA can maintain the GSH level by direct reduction of GSSG and promotion of cysteine uptake that would decrease the ratio of cystine to cysteine and improve GSH synthesis [31]. Results of our model experiments demonstrated that DHLA reduced the pro-ferroptotic HpETE-PE to HETE-PE, providing direct evidence for the role of DHLA in the elimination of ferroptotic phospholipid signals. Dihydrolipoyl residues localized on KGDH and PDH can also participate in the regulation of ferroptosis through ROS production by these enzymes. During the catalytic cycle of α-keto acid dehydrogenase, dihydrolipoamide localized on E2 subunits serves as a shuttle reducing the E3-bound FAD^+ and, $FADH_2$ formed in this reaction further generates NADH through coupled oxidation-reduction reactions with NAD^+. When the availability of NAD^+ is diminished, $FADH_2$ can be readily oxidized by O_2 generating a semiquinone and superoxide. As a result, the enzyme loses its activity, generates superoxide, and enhances mtROS levels leading to ferroptosis [32]. Genetic inhibition of dihydrolipoyl dehydrogenase (DLD), an E3 component of the KGDH complex that accepts electrons from the E2 bound dihydrolipoyl residue, inhibited ferroptosis in head and neck cancer cells induced by sulfasalazine-dependent inhibition of system x_c^-. Upregulation of the E3 in these cells markedly increased lipid peroxidation and mitochondrial iron accumulation suggesting that dihydrolipoyl residue of KGDH can be involved in mitochondrial ferroptotic signaling [33].

Recent studies also demonstrated the role of dihydrolipoyl residue of PDH in ROS generation and ferroptosis. In contrast to KGDH, silencing of the E3 subunit of PDH increased the pro-ferroptotic effect of either glucose or its metabolite pyruvate, while downregulation of the E1 subunit, which catalyzes the first step of the overall process, has an anti-ferroptotic effect [34]. This study suggested non-enzymatic oxidation (autoxidation) of DHLA that is known to produce superoxide [11,35]. Thus, high ROS production and DHLA oxidation in response to ferroptotic stimuli could enhance GSH depletion leading to cell death and conversely, the addition of free DHLA could prevent KGDH-induced ROS generation [36] and thus, inhibit ferroptosis. In addition to its effects on GSH metabolism, DHLA was shown to inhibit 15LOX, an enzyme that oxidizes generation of ferroptotic PEox species when complexed with PEBP1 through reduction of Fe^{3+} to Fe^{2+} at the catalytic site of the enzyme [37]. In line with this, our data show that DHLA can directly eliminate ferroptotic PEox species *in vitro* (Fig. 5B–D).

GSH, a highly important ubiquitous tripeptide produced by most mammalian cells, is one of the main mechanisms of the antioxidant defense system against ROS and electrophiles. Lack of enzymes for GSH synthesis, in addition to a net negative charge of GSH at physiological pH and a high concentration in mitochondria, implies a facilitated transport mechanism for the GSH transport into the mitochondria [13,16]. In mammalian cells, the mitochondrial carrier proteins represent a large SLC25 family of nuclear-encoded transporters in the IMM that account for over 60 proteins, and only about half of them have been functionally characterized [38]. Among the carrier proteins, only eight

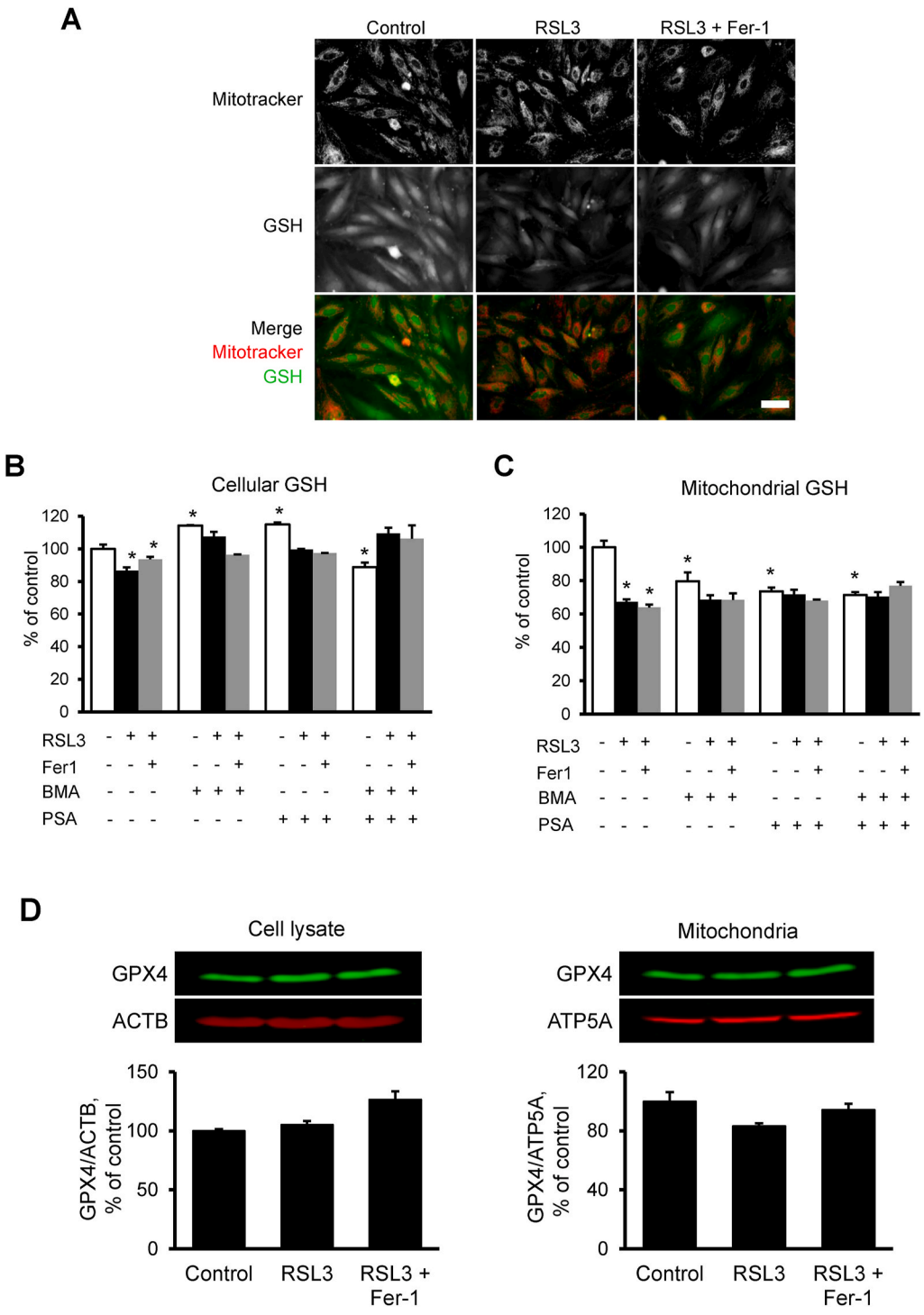

Fig. 7. The effects of ferroptosis on GSH and GPX4 levels. ***A,*** H9c2 cells exposed to 0.5 μM RSL3 in the presence or absence of Fer-1 (2 μM) for 1 h were stained with 50 nM Mitotracker (for staining of mitochondria) for 1 h and 10 μM Thiol Fluorescent Probe IV (for staining of GSH) for 10 min. Bar = 100 μm. ***B,C,*** Cellular and mitochondrial GSH levels. Cells were treated with 0.5 μM RSL3 in the presence or absence of Fer-1 (2 μM), BMA (5 mM), and PSA (5 mM) for 18 h $^{*}p < 0.01$ vs. control; n = 3 per group. ***D,*** GPX4 protein levels in cell lysates and mitochondria isolated from control and RSL3 (0.5 μM) challenged cells that were incubated in the presence or absence of Fer-1 (2 μM) for 1 h. Representative immunoblots are shown at the top of each graph. An equal amount of protein (20 μg) was loaded into each well. Proteins were separated by SDS-PAGE and identified by Western blotting using specific antibodies. GPX4 levels were normalized to β-actin (ACTB, for cell lysate) and ATP5A (for mitochondria).

are anion carriers and can potentially participate in GSH transport across the IMM [39]. Initial studies identified the capability of two carriers, DIC and OGC to transport GSH in isolated human kidney mitochondria and mitoplasts wherein pharmacological inhibition of DIC and OGC hampered GSH transport [17,18]. The contribution of DIC to GSH transport was confirmed in cancer cells, where artificially increased GSH levels in mitochondria by a mitochondria-permeable glutathione-ethyl ester was prevented by DIC inhibition thereby, implicating that DIC participates in GSH uptake [40]. High vulnerability of neurons to oxidative and nitrosative stressors was prevented by incubation with a cell-permeable derivative of GSH monoethyl ester but not malate, and genetic knockdown of DIC enhanced the vulnerability of neurons to oxidative stress [41]. On the other hand, elucidation of GSH transport by using fused membrane vesicles of *Lactococcus lactis* overexpressing the DIC and OGC found that these mitochondrial carriers could not transport GSH measured directly [19]. Thus, the identity of the mitochondrial GSH transporter(s) remains elusive and the role of DIC and OGC in GSH transport is still controversial; multiple low-affinity IMM carriers that typically transport alternative substrates may participate in GSH transport in mammalian mitochondria.

In our studies, inhibition of DIC and OGC reduced GSH levels in mitochondria (Fig. 7C) suggesting the role of these carriers in GSH

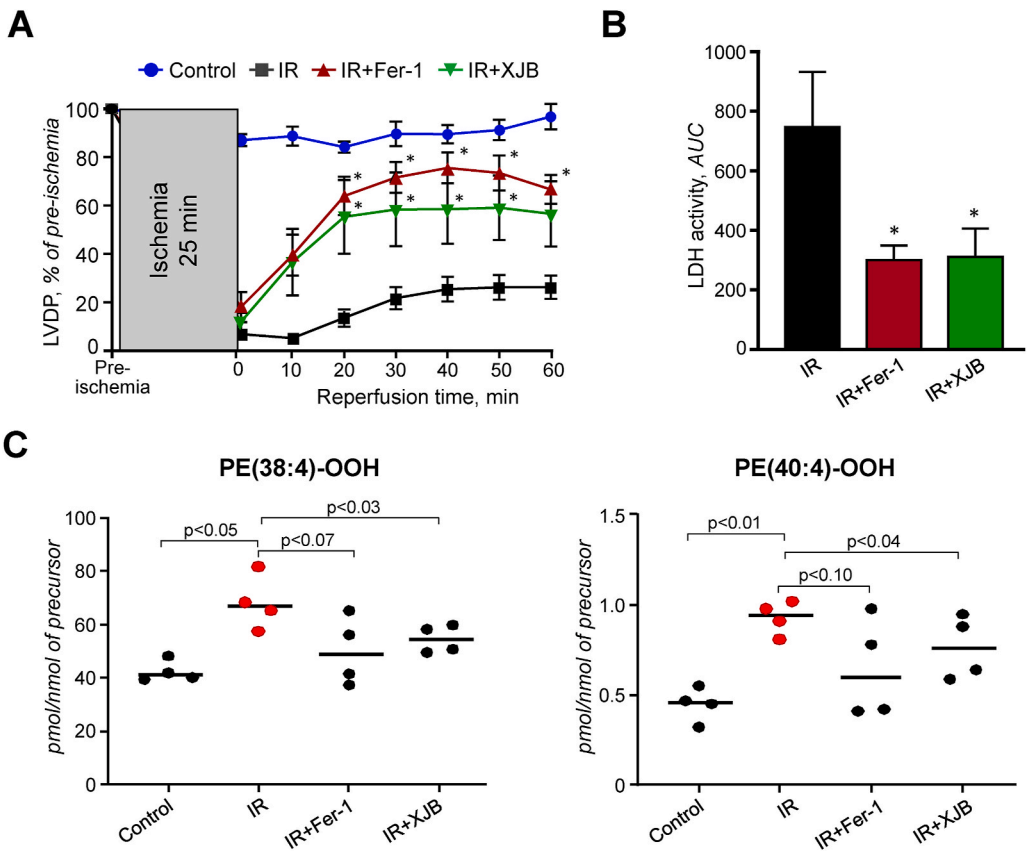

Fig. 8. Cardiac IR-induced accumulation of ferroptotic PE species in mitochondria. Langendorff-perfused rat hearts were subjected to global ischemia for 25 min followed by 60-min reperfusion in the presence or absence of Fer-1 and XJB-5-131 (XJB, a mitochondria-targeted ROS and electron scavenger). Fer-1 (1 μM) and XJB (0.2 μM) dissolved in DMSO were present in the perfusion buffer 10 min before ischemia and throughout the entire reperfusion period. ***A,*** Left ventricular (LV) developed pressure (LVDP) calculated as the difference between LV systolic and end-diastolic pressures and presented as a percentage of pre-ischemic values. ***B,*** LDH activity was measured in the coronary effluent during the reperfusion period and presented as the area under the curve (AUC). *$p < 0.05$ vs IR group. n = 7–8. ***C***, Levels of the PEox species PE(38:4)-OOH (*left panel*) and PE(40:4)-OOH (*right panel*) in cardiac mitochondria. Precursors for PE(38:4)-OOH and PE(40:4)-OOH are PE(38:4) and PE (40:4), respectively. Data are presented as pmol of oxidized PE per μmol of precursor PE. n = 4 per each group.

transport. However, DIC and OGC inhibition could reduce mitochondrial GSH levels through other mechanisms independently of its transport. The carriers are involved in mitochondrial metabolism; they transport dicarboxylates (2-oxoglutarate, malate, and succinate), the intermediates for the TCA cycle. Also, the transport of the dicarboxylates is important for the maintenance of homeostasis and metabolism of other metabolites in mitochondria such as glutamate, isocitrate, pyruvate, and oxaloacetate, among others. Hence, inhibition of DIC and OGC could diminish the activity of TCA cycle enzymes and PDH leading to increased mtROS production [35,42]. Estimated levels of superoxide anion in mitochondria are 5-10-fold higher than in the cytosol [43], and a powerful antioxidant system in mitochondria including, among others, superoxide dismutase, catalase, GPX, thioredoxin system, and GSH, prevents mtROS accumulation under physiological conditions. Accordingly, inhibition of ETC complexes, particularly, complexes I and III significantly increased cell death in response to RSL3 (Fig. 3). This can be explained by mitochondrial GSH depletion due to high mtROS production at these complexes [25]. Low GSH levels in mitochondria could also affect the S-glutathionylation of mitochondrial proteins particularly ETC complexes and TCA cycle enzymes [10,44], and diminish their activity. This feedback loop could further enhance ROS production and GSH depletion in mitochondria. Notably, loss of GSH has been shown to provoke the opening of the mitochondrial permeability transition pores, non-selective pathological channels in the IMM [45,46]. Opening of the pores is accompanied by the loss of $\Delta\Psi_m$ and a dramatic increase of mtROS production resulting in mitochondrial swelling and initiation of mitochondria-mediated cell death. Thus, high mtROS due to inhibition of DIC and OGC could enhance GSH depletion and alter mitochondrial redox homeostasis even in the absence of the capability of these carriers to transport GSH.

Cell death induced by RSL3 was aggravated in the presence of inhibitors for ETC complexes I and III, and mostly for OXPHOS (Fig. 3). Previous studies demonstrated protective effects of ETC inhibition on erastin- or cysteine deprivation (CD)-induced ferroptosis in mouse embryonic fibroblasts that were associated with accumulation of lipid peroxides [7]. Interestingly, no significant effects of antimycin A and FCCP on erastin-induced ferroptosis were found in HT-1080 cells [34]. The opposite effects of ETC and OXPHOS inhibition on cell death induced by RSL3 and erastin/CD can be explained by the differences in the mechanisms of action of these ferroptotic factors as well as in cell types (cancer vs. non-cancer cells). RSL3 blocks the final step in the production of PEox; it binds to and inactivates GPX4, and thus, results in the accumulation of peroxidized PE species whereas erastin/CD compromise GSH synthesis required for the GPX4 activity. Erastin and CD have been shown to induce hyperpolarization of the IMM associated with high mtROS production that, in turn, can deplete GSH levels and compromise mitochondrial function leading to cell death.

5. Conclusion

Coronary heart diseases such as myocardial infarction/IR injury trigger multiple forms of programmed cell death [47], and hence, it is important to identify the specific cell death program(s) preferably occur in the myocardium with the progression of post-infarction remodeling to design optimized mechanism-based cardioprotective strategies [48]. The present study revealed an early response of cardiac mitochondria to ferroptotic stimulus associated with accumulation of ferroptotic phospholipid signals, particularly PEox, in mitochondria during cardiac IR injury or after treatment of H9c2 cardiomyoblasts with RSL3. Maintenance of the mitochondrial GSH pool is important for the prevention of ferroptosis in cardiomyocytes.

Author contributions

Conception and design: Sa.J, V.E.K, H.B; Acquisition of data: Se.J, X. R.C, Y.Y.T, C.M.S, A.A.K, V.A.T; analysis and interpretation of data: Se.J,

X.R.C, Y.Y.T, C.M.S, A.A.K, V.A.T; writing, review, and/or revision of the manuscript: Sa.J, V.E.K, H.B; administrative, technical, or material support: Sa.J, V.E.K, H.B.

Declaration of competing interest

The authors declare no competing financial interests.

Acknowledgments

This study was supported by NIH grants: SC1GM128210, R25GM061838, HL114453, AI156924, AI156923, CA165065, CA243142, AI145406, NS076511, and NS061817. The authors thank Dr. Peter Wipf from the University of Pittsburgh for providing XJB-5-131.

References

[1] W.S. Yang, R. SriRamaratnam, M.E. Welsch, K. Shimada, R. Skouta, V. S. Viswanathan, J.H. Cheah, P.A. Clemons, A.F. Shamji, C.B. Clish, L.M. Brown, A. W. Girotti, V.W. Cornish, S.L. Schreiber, B.R. Stockwell, Regulation of ferroptotic cancer cell death by GPX4, Cell 156 (1–2) (2014) 317–331.

[2] S.J. Dixon, K.M. Lemberg, M.R. Lamprecht, R. Skouta, E.M. Zaitsev, C.E. Gleason, D.N. Patel, A.J. Bauer, A.M. Cantley, W.S. Yang, B. Morrison 3rd, B.R. Stockwell, Ferroptosis: an iron-dependent form of nonapoptotic cell death, Cell 149 (5) (2012) 1060–1072.

[3] V.E. Kagan, G. Mao, F. Qu, J.P. Angeli, S. Doll, C.S. Croix, H.H. Dar, B. Liu, V. A. Tyurin, V.B. Ritov, A.A. Kapralov, A.A. Amoscato, J. Jiang, T. Anthonymuthu, D. Mohammadyani, Q. Yang, B. Proneth, J. Klein-Seetharaman, S. Watkins, I. Bahar, J. Greenberger, R.K. Mallampalli, B.R. Stockwell, Y.Y. Tyurina, M. Conrad, H. Bayir, Oxidized arachidonic and adrenic PEs navigate cells to ferroptosis, Nat. Chem. Biol. 13 (1) (2017) 81–90.

[4] S.E. Wenzel, Y.Y. Tyurina, J. Zhao, C.M. St Croix, H.H. Dar, G. Mao, V.A. Tyurin, T. S. Anthonymuthu, A.A. Kapralov, A.A. Amoscato, K. Mikulska-Ruminska, I. H. Shrivastava, E.M. Kenny, Q. Yang, J.C. Rosenbaum, L.J. Sparvero, D.R. Emlet, X. Wen, Y. Minami, F. Qu, S.C. Watkins, T.R. Holman, A.P. VanDemark, J. A. Kellum, I. Bahar, H. Bayir, V.E. Kagan, PEBP1 wardens ferroptosis by enabling lipoxygenase generation of lipid death signals, Cell 171 (3) (2017) 628–641 e26.

[5] S. Toppo, L. Flohe, F. Ursini, S. Vanin, M. Maiorino, Catalytic mechanisms and specificities of glutathione peroxidases: variations of a basic scheme, Biochim. Biophys. Acta 1790 (11) (2009) 1486–1500.

[6] J.P. Friedmann Angeli, M. Schneider, B. Proneth, Y.Y. Tyurina, V.A. Tyurin, V. J. Hammond, N. Herbach, M. Aichler, A. Walch, E. Eggenhofer, D. Basavarajappa, O. Rådmark, S. Kobayashi, T. Seibt, H. Beck, F. Neff, I. Esposito, R. Wanke, H. Förster, O. Yefremova, M. Heinrichmeyer, G.W. Bornkamm, E.K. Geissler, S. B. Thomas, B.R. Stockwell, V.B. O'Donnell, V.E. Kagan, J.A. Schick, M. Conrad, Inactivation of the ferroptosis regulator Gpx4 triggers acute renal failure in mice, Nat. Cell Biol. 16 (12) (2014) 1180–1191.

[7] M. Gao, J. Yi, J. Zhu, A.M. Minikes, P. Monian, C.B. Thompson, X. Jiang, Role of mitochondria in ferroptosis, Mol Cell 73 (2) (2019) 354–363, e3.

[8] M. Gao, P. Monian, N. Quadri, R. Ramasamy, X. Jiang, Glutaminolysis and transferrin regulate ferroptosis, Mol Cell 59 (2) (2015) 298–308.

[9] A.L. McLain, P.A. Szweda, L.I. Szweda, alpha-Ketoglutarate dehydrogenase: a mitochondrial redox sensor, Free Radic. Res. 45 (1) (2011) 29–36.

[10] M.A. Applegate, K.M. Humphries, L.I. Szweda, Reversible inhibition of alpha-ketoglutarate dehydrogenase by hydrogen peroxide: glutathionylation and protection of lipoic acid, Biochemistry 47 (1) (2008) 473–478.

[11] C.L. Quinlan, R.L. Goncalves, M. Hey-Mogensen, N. Yadava, V.I. Bunik, M. D. Brand, The 2-oxoacid dehydrogenase complexes in mitochondria can produce superoxide/hydrogen peroxide at much higher rates than complex I, J. Biol. Chem. 289 (12) (2014) 8312–8325.

[12] G. Camiolo, D. Tibullo, C. Giallongo, A. Romano, N.L. Parrinello, G. Musumeci, M. Di Rosa, N. Vicario, M.V. Brundo, F. Amenta, M. Ferrante, C. Copat, R. Avola, G. Li Volti, A. Salvaggio, F. Di Raimondo, G.A. Palumbo, Alpha-lipoic acid reduces iron-induced toxicity and oxidative stress in a model of iron overload, Int. J. Mol. Sci. 20 (3) (2019).

[13] M. Marí, A. Morales, A. Colell, C. García-Ruiz, J.C. Fernández-Checa, Mitochondrial glutathione, a key survival antioxidant, Antioxidants Redox Signal. 11 (11) (2009) 2685–2700.

[14] M. Marí, A. Colell, A. Morales, C. von Montfort, C. Garcia-Ruiz, J.C. Fernández-Checa, Redox control of liver function in health and disease, Antioxidants Redox Signal. 12 (11) (2010) 1295–1331.

[15] V. Ribas, C. García-Ruiz, J.C. Fernández-Checa, Glutathione and mitochondria, Front. Pharmacol. 5 (2014) 151.

[16] O.W. Griffith, A. Meister, Origin and turnover of mitochondrial glutathione, Proc. Natl. Acad. Sci. U. S. A. 82 (14) (1985) 4668–4672.

[17] Z. Chen, D.A. Putt, L.H. Lash, Enrichment and functional reconstitution of glutathione transport activity from rabbit kidney mitochondria: further evidence for the role of the dicarboxylate and 2-oxoglutarate carriers in mitochondrial glutathione transport, Arch. Biochem. Biophys. 373 (1) (2000) 193–202.

[18] Z. Chen, L.H. Lash, Evidence for mitochondrial uptake of glutathione by dicarboxylate and 2-oxoglutarate carriers, J. Pharmacol. Exp. Therapeut. 285 (2) (1998) 608–618.

[19] L.M. Booty, M.S. King, C. Thangaratnarajah, H. Majd, A.M. James, E.R. Kunji, M. P. Murphy, The mitochondrial dicarboxylate and 2-oxoglutarate carriers do not transport glutathione, FEBS Lett. 589 (5) (2015) 621–628.

[20] S. Mizuarai, S. Miki, H. Araki, K. Takahashi, H. Kotani, Identification of dicarboxylate carrier Slc25a10 as malate transporter in de novo fatty acid synthesis, J. Biol. Chem. 280 (37) (2005) 32434–32441.

[21] S. Jang, T.S. Lewis, C. Powers, Z. Khuchua, C.P. Baines, P. Wipf, S. Javadov, Elucidating mitochondrial electron transport chain supercomplexes in the heart during ischemia-reperfusion, Antioxidants Redox Signal. 27 (1) (2017) 57–69.

[22] K.M. Rodriguez-Graciani, X.R. Chapa-Dubocq, L.A. MacMillan-Crow, S. Javadov, Association between L-OPA1 cleavage and cardiac dysfunction during ischemia-reperfusion injury in rats, Cell. Physiol. Biochem. 54 (6) (2020) 1101–1114.

[23] C.A. Schneider, W.S. Rasband, K.W. Eliceiri, NIH Image to ImageJ: 25 years of image analysis, Nat. Methods 9 (7) (2012) 671–675.

[24] R.M. Parodi-Rullán, X. Chapa-Dubocq, R. Guzmán-Hernández, S. Jang, C.A. Torres-Ramos, S. Ayala-Peña, S. Javadov, The role of adenine nucleotide translocase in the assembly of respiratory supercomplexes in cardiac cells, Cells 8 (10) (2019).

[25] S. Jang, S. Javadov, Elucidating the contribution of ETC complexes I and II to the respirasome formation in cardiac mitochondria, Sci. Rep. 8 (1) (2018) 17732.

[26] L.J. Sparvero, H. Tian, A.A. Amoscato, W.Y. Sun, T.S. Anthonymuthu, Y.Y. Tyurina, O. Kapralov, S. Javadov, R.R. He, S.C. Watkins, N. Winograd, V.E. Kagan, H. Bayir, Direct mapping of phospholipid ferroptotic death signals in cells and tissues by gas cluster ion beam secondary ion mass spectrometry (GCIB-SIMS), Angew Chem. Int. Ed. Engl. 60 (21) (2021) 11784–11788.

[27] M.M. Gaschler, A.A. Andia, H. Liu, J.M. Csuka, B. Hurlocker, C.A. Vaiana, D. W. Heindel, D.S. Zuckerman, P.H. Bos, E. Reznik, L.F. Ye, Y.Y. Tyurina, A.J. Lin, M. S. Shchepinov, A.Y. Chan, E. Peguero-Pereira, M.A. Fomich, J.D. Daniels, A. V. Bekish, V.V. Shmanai, V.E. Kagan, L.K. Mahal, K.A. Woerpel, B.R. Stockwell, FINO2 initiates ferroptosis through GPX4 inactivation and iron oxidation, Nat. Chem. Biol. 14 (5) (2018) 507–515.

[28] N. Escobales, R.E. Nunez, S. Jang, R. Parodi-Rullan, S. Ayala-Pena, J.R. Sacher, E. M. Skoda, P. Wipf, W. Frontera, S. Javadov, Mitochondria-targeted ROS scavenger improves post-ischemic recovery of cardiac function and attenuates mitochondrial abnormalities in aged rats, J. Mol. Cell. Cardiol. 77 (2014) 136–146.

[29] T. Krainz, M.M. Gaschler, C. Lim, J.R. Sacher, B.R. Stockwell, P. Wipf, A mitochondrial-targeted nitroxide is a potent inhibitor of ferroptosis, ACS Cent. Sci. 2 (9) (2016) 653–659.

[30] J.J. Maguire, Y.Y. Tyurina, D. Mohammadyani, A.A. Kapralov, T.S. Anthonymuthu, F. Qu, A.A. Amoscato, L.J. Sparvero, V.A. Tyurin, J. Planas-Iglesias, R.R. He, J. Klein-Seetharaman, H. Bayir, V.E. Kagan, Known unknowns of cardiolipin signaling: the best is yet to come, Biochim. Biophys. Acta Mol. Cell Biol. Lipids 1862 (1) (2017) 8–24.

[31] S. Golbidi, M. Badran, I. Laher, Diabetes and alpha lipoic Acid, Front. Pharmacol. 2 (2011) 69.

[32] V.I. Bunik, Redox-driven signaling: 2-oxo acid dehydrogenase complexes as sensors and transmitters of metabolic imbalance, Antioxidants Redox Signal. 30 (16) (2019) 1911–1947.

[33] D. Shin, J. Lee, J.H. You, D. Kim, J.L. Roh, Dihydrolipoamide dehydrogenase regulates cystine deprivation-induced ferroptosis in head and neck cancer, Redox Biol 30 (2020) 101418.

[34] A.M. Vuckovic, R. Venerando, E. Tibaldi, V. Bosello Travain, A. Roveri, L. Bordin, G. Miotto, G. Cozza, S. Toppo, M. Maiorino, F. Ursini, Aerobic pyruvate metabolism sensitizes cells to ferroptosis primed by GSH depletion, Free Radic. Biol. Med. 167 (2021) 45–53.

[35] V.I. Bunik, M.D. Brand, Generation of superoxide and hydrogen peroxide by side reactions of mitochondrial 2-oxoacid dehydrogenase complexes in isolation and in cells, Biol. Chem. 399 (5) (2018) 407–420.

[36] A. Ambrus, L. Tretter, V. Adam-Vizi, Inhibition of the alpha-ketoglutarate dehydrogenase-mediated reactive oxygen species generation by lipoic acid, J. Neurochem. 109 (Suppl 1) (2009) 222–229.

[37] D. Lapenna, G. Ciofani, S.D. Pierdomenico, M.A. Giamberardino, F. Cuccurullo, Dihydrolipoic acid inhibits 15-lipoxygenase-dependent lipid peroxidation, Free Radic. Biol. Med. 35 (10) (2003) 1203–1209.

[38] F. Palmieri, The mitochondrial transporter family SLC25: identification, properties and physiopathology, Mol. Aspect. Med. 34 (2–3) (2013) 465–484.

[39] L.H. Lash, Mitochondrial glutathione transport: physiological, pathological and toxicological implications, Chem. Biol. Interact. 163 (1–2) (2006) 54–67.

[40] J. Hlouschek, V. Ritter, F. Wirsdorfer, D. Klein, V. Jendrossek, J. Matschke, Targeting SLC25A10 alleviates improved antioxidant capacity and associated radioresistance of cancer cells induced by chronic-cycling hypoxia, Canc. Lett. 439 (2018) 24–38.

[41] H.M. Wilkins, D. Kirchhof, E. Manning, J.W. Joseph, D.A. Linseman, Mitochondrial glutathione transport is a key determinant of neuronal susceptibility to oxidative and nitrosative stress, J. Biol. Chem. 288 (7) (2013) 5091–5101.

[42] E.T. Chouchani, V.R. Pell, E. Gaude, D. Aksentijevic, S.Y. Sundier, E.L. Robb, A. Logan, S.M. Nadtochiy, E.N.J. Ord, A.C. Smith, F. Eyassu, R. Shirley, C.H. Hu, A. J. Dare, A.M. James, S. Rogatti, R.C. Hartley, S. Eaton, A.S.H. Costa, P.S. Brookes, S.M. Davidson, M.R. Duchen, K. Saeb-Parsy, M.J. Shattock, A.J. Robinson, L. M. Work, C. Frezza, T. Krieg, M.P. Murphy, Ischaemic accumulation of succinate controls reperfusion injury through mitochondrial ROS, Nature 515 (7527) (2014) 431–435.

[43] E. Cadenas, K.J. Davies, Mitochondrial free radical generation, oxidative stress, and aging, Free Radic. Biol. Med. 29 (3–4) (2000) 222–230.

[44] J. Garcia, D. Han, H. Sancheti, L.P. Yap, N. Kaplowitz, E. Cadenas, Regulation of mitochondrial glutathione redox status and protein glutathionylation by respiratory substrates, J. Biol. Chem. 285 (51) (2010) 39646–39654.
[45] M.K. Savage, D.J. Reed, Release of mitochondrial glutathione and calcium by a cyclosporin A-sensitive mechanism occurs without large amplitude swelling, Arch. Biochem. Biophys. 315 (1) (1994) 142–152.
[46] B.V. Chernyak, P. Bernardi, The mitochondrial permeability transition pore is modulated by oxidative agents through both pyridine nucleotides and glutathione at two separate sites, Eur. J. Biochem. 238 (3) (1996) 623–630.
[47] D.P. Del Re, D. Amgalan, A. Linkermann, Q. Liu, R.N. Kitsis, Fundamental mechanisms of regulated cell death and implications for heart disease, Physiol. Rev. 99 (4) (2019) 1765–1817.
[48] P.K. Mishra, A. Adameova, J.A. Hill, C.P. Baines, P.M. Kang, J.M. Downey, J. Narula, M. Takahashi, A. Abbate, H.C. Piristine, S. Kar, S. Su, J.K. Higa, N. K. Kawasaki, T. Matsui, Guidelines for evaluating myocardial cell death, Am. J. Physiol. Heart Circ. Physiol. 317 (5) (2019) H891–h922.